HHS Public Access

Author manuscript

Biochemistry. Author manuscript; available in PMC 2017 October 04.

Published in final edited form as:

Biochemistry. 2016 October 04; 55(39): 5587–5594. doi:10.1021/acs.biochem.6b00786.

Targeting Bacterial Nitric Oxide Synthase with Aminoquinoline-based Inhibitors

Jeffrey K. Holden[1], **Matthew C. Lewis**[1], **Maris A. Cinelli**[4,5], **Ziad Abdullatif**[1], **Anthony V. Pensa**[4,5], **Richard B. Silverman**[4,5,6,*], and **Thomas L. Poulos**[1,2,3,*]

[1]Department of Molecular Biology and Biochemistry, University of California, Irvine, CA 92697-3900

[2]Department of Pharmaceutical Sciences, University of California, Irvine, CA 92697-3900

[3]Department of Chemistry, University of California, Irvine, CA 92697-3900

[4]Department of Chemistry and Molecular Biosciences, Northwestern University, Evanston, IL 60208-3113

[5]Department of Chemistry of Life Processes Institute, Northwestern University, Evanston, IL 60208-3113

[6]Center for Molecular Innovation and Drug Discovery, Northwestern University, Evanston, IL 60208-3113

Abstract

Nitric oxide (NO) is produced in Gram-positive pathogens *Bacillus anthracis* and *Staphylococcus aureus* by the bacterial isoform of nitric oxide synthase (NOS). Inhibition of bacterial nitric oxide synthase (bNOS) has been identified as a promising antibacterial strategy for targeting methicillin-resistant *Staphylocoocus aureus*[1]. One class of NOS inhibitors that demonstrates antimicrobial efficacy utilizes an aminoquinoline scaffold. Here we report on a variety of aminoquinolines that target the bacterial NOS active site, in part, by binding to a hydrophobic patch that is unique to bNOS. Through mutagenesis and crystallographic studies, our findings demonstrate that aminoquinolines are an excellent scaffold to further aid in the development of bNOS-specific inhibitors.

Graphical abstract

*To whom correspondence should be addressed. T.L.P.: poulos@uci.edu; phone, (949) 824-7020; fax, (949) 824-3280. R.B.S.: Agman@chem.northwestern.edu; phone, (847) 491-5653; fax, (847) 491-7713.

‡Coordinates and structure factors have been deposited in the Protein Data Base under accession numbers 5G65, 5G66, 5G67, 5G68, 5G69, 5G6A, 5G6B, 5G6C, 5G6D, 5G6E, 5G6F, 5G6G, 5G6H, 5G6I, 5G6J, 5G6K, 5G6L, 5G6M, 5G6N, 5G6O, 5G6P, 5G6Q.

Supporting Information

A summary of crystallographic and refinement statistics are provided in Table S1 and the electron density map for various inhibitors in Fig. S1.

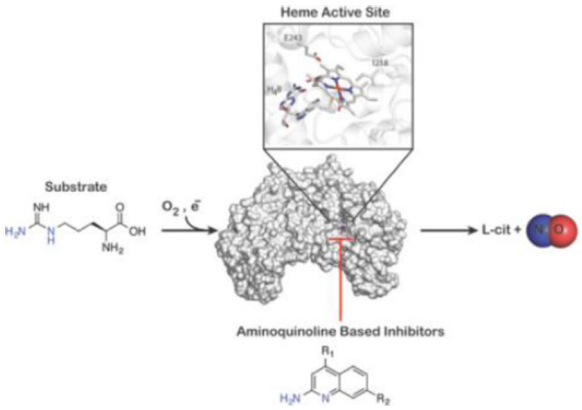

Bacterial nitric oxide synthase (bNOS) shares many structural and enzymatic properties with the mammalian nitric oxide synthases (mNOS), neuronal NOS, inducible NOS, and endothelial NOS. Both bNOS and mNOS have heme-containing oxygenase domains that produce the free radical gas nitric oxide (NO) through a multi-electron transfer process. Biosynthesis of NO requires the substrate L-arginine (L-Arg), NADPH-derived electrons, and a reduced pterin group[2]. The active sites of all NOS isoforms are very similar and they all bind L-Arg directly over the heme, where a conserved L-Glu residue holds the L-Arg in place[3]. Despite many similarities between mNOS and bNOS, there are some significant differences. The mNOS isoforms are multi-domain proteins that transfer electrons from NADPH to the oxygenase domain *via* a separate reductase domain. Most bNOS enzymes, however, are composed of only the oxygenase domain, and thus depend on other redox partners for electron transfer[4]. The mNOS isoforms also contain an N-terminal Zn^{2+} binding motif that helps stabilize the dimer interface and binding of the pterin cofactor, tetrahydrobiopterin. In sharp contrast, bNOS lacks the Zn^{2+} binding motif and therefore has a more open dimer interface[5,6] resulting in a larger pterin binding pocket[7,8].

One of the many proposed roles of NO in bacteria is to help protect the bacteria from host cell or antibiotic-induced oxidative stress[9,10], and in *Staphylococcus aureus* NO facilitates bacterial virulence[11].Owing to the important role NO plays in methicillin-resistant *S. aureus* (MRSA), bNOS has become a promising therapeutic target. Previously, we demonstrated that NOS inhibitors improve the efficacy of the antimicrobial acriflavine[12,13] and hydrogen peroxide-derived oxidative stress[1]. From our previous studies on NOS inhibition, we have identified several key active site differences that can be exploited for the design of bNOS specific inhibitors. Most notable is the “open” pterin-binding site that is unique to bNOS isoforms because of the missing Zn^{2+} binding motif[12] found in mNOS isoforms. Another notable difference is a hydrophobic patch at the distal face of the heme active site[1]; in bNOS this patch is composed of a L-Ile residue, and in mNOS isoforms the analogous residue is a L-Val.

From a chemically diverse library of nNOS inhibitors, aminoquinoline-based inhibitors were identified for further development of a bNOS specific inhibitor targeting MRSA[1]. The aminoquinoline inhibitors were found to bind to the bNOS active site and exploit the hydrophobic patch contributed by the L-Ile residue (L-Val in mNOS) through van der Waals

interactions. Since the aminoquinoline class of NOS inhibitors presents promising antimicrobial effects against MRSA, further characterization of aminoquinolines as bNOS inhibitors is necessary. Here we report on the characterization of 17 aminoquinoline-based bNOS inhibitors using binding, inhibition, and crystallographic studies. The inhibitors reported herein are shown in Figure 1.

Experimental Procedures

Molecular Biology

Bacillus subtilis NOS (bsNOS) DNA was previously cloned into a pET28a (Novagen) expression plasmid[12] with surface entropy reduction mutations E24A/E25A/E316A identified using the sERP server[14]. Introduction and expression/purification of bsNOS I218V was previously described[1]. Codon optimized DNA for *E. coli* expression of *Homo sapiens* inducible NOS (iNOS) was synthesized by Genewiz (South Plainfield, NJ) and cloned into pET28a (Novagen) using NdeI and XhoI as the restriction sites. The iNOS heme domain expression construct encoded residues Arg83 to Arg536. Active site mutation V352I was introduced to the heme domain expression construct by site directed mutagenesis using PfuTurbo (Agilent). An N-terminal His-tag calmodulin-expressing construct was prepared by PCR amplification of the calmodulin gene from a previous calmodulin expressing construct (a kind gift from Prof. Paul Ortiz de Montellano, UCSF) and cloned into pET28a (Novagen) using restriction sites NheI and HindIII, resulting in plasmid pJH114. Expression plasmid pJH114 was then digested with restriction enzymes XbaI and XhoI. The digested insert containing the calmodulin encoded gene was ligated into the XbaI and XhoI restriction sites of pET21a (Novagen) to produce Calmodulin expression plasmid pJH115.

Expression and Purification

Both bsNOS and I218V bsNOS were overexpressed in *Escherichia coli* BL21(DE3) and isolated as previously described[12,15]. Expression of the iNOS heme domain required co-expression with calmodulin. Hence, the iNOS heme domain-expressing plasmid was co-transformed with calmodulin expressing plasmid pJH115 into Overexpress C41(DE3) chemically competent *E. coli* cells (Sigma-Aldrich). The following morning an individual colony was inoculated into 5 mL of LB media supplemented with ampicillin and kanamycin at 50 ng/mL and 35 ng/mL, respectively. The starter culture was then aliquoted to 1 L TB media supplemented with 500 μM $CaCl_2$, 50 ng/mL ampicillin, and 35 ng/mL kanamycin. Following inoculation of the media, the culture was shaken overnight at 200 RPM and 30 °C. After this period, the culture reached OD_{600} > 2.0 and was induced by addition of 400 μM δ-aminolevulinic acid and 0.5 mM isopropyl β-D-1-thiogalactopyranoside. The bacterial cells were harvested by centrifugation and resuspended in lysis buffer composed of 40 mM Bis-Tris methane (pH 7.0), 200 mM NaCl, 1 mM $CaCl_2$, 4 mM L-Arg, 5 μM H_4B, 10% glycerol, and 5 mM imidazole. The bacterial cells were lysed using a microfluidics M-110L microfluidizer, and cell debris removed by centrifugation prior to loading on to a Ni^{2+}-nitrilotriacetate affinity column. The column was then washed with 10 CV of lysis buffer supplemented with 15 mM imidazole, and the targeted proteins were eluted with lysis buffer supplemented with 250 mM imidazole. The N-terminal His tag was removed by the protease thrombin (MP Biomedicals) at 4 °C overnight. Cleaved protein was resolved from

the non-cleaved protein by Ni^{2+}-nitrilotriacetate affinity chromatography. The iNOS/calmodulin protein complex was further purified by Sepharose size-exclusion chromatography using a buffer composed of 40 mM HEPES (pH 7.6), 200 mM NaCl, 10% v/v glycerol, 10 μM H_4B, 0.5 mM imidazole, and 3 mM dithiothreitol.

Imidazole Displacement

The sample absorbance was monitored using a Cary 3E UV-visible spectrophotometer as inhibitors were titrated into a cuvette containing 50 mM Tris (pH 7.4), 1 mM imidazole, 100 μM dithiothreitol, 10 mM NaCl, and 2 μM of the corresponding NOS. The difference in the imidazole-bound low-spin state and the inhibitor-bound high-spin state was calculated as a function of inhibitor concentration, as previously annotated for bsNOS, bsNOS I218V, iNOS, and iNOS V352I[16]. From these data $K_{S,app}$, was calculated from the concentration of inhibitor required to transition 50% of the sample from low-spin to high-spin and was determined as previously reported[12] using a nonlinear regression analysis available in Sigmaplot version 10.0 (Systat Software, Inc., www.sigmaplot.com). The K_S for each ligand was then calculated from the $K_{S,app}$ as previously described[17] using the K_D of imidazole to bsNOS, bsNOS I218V, iNOS and iNOS 352I[16].

IC_{50} Determination

Enzyme activity for bsNOS was measured using the previously described bBidomain construct.[15] The bBidomain enzyme is a fusion protein composed of bsNOS at the N-terminus, flavoprotein YkuN at the C-terminus, and a 30 amino acid peptide linker between the two proteins. In the presence of reductase YumC and NADPH a catalytic system is established and electrons are transferred to the bBidomain active site *via* the flavoproteins. Enzyme activity was measured by Griess reaction as previously described.[15] To calculate the IC_{50}, nitrite levels were measured at varying concentrations of inhibitor ranging from 0.1 μM to 200 μM for three separate replicates. The average percent inhibition was calculated for each inhibitor concentration evaluated and a curve was fit to the data in Sigmaplot version 10.0 (Systat Software, Inc., www.sigmaplot.com). The IC_{50} was extrapolated from the curve generated by Sigmaplot version 10.0.

Crystallization and Sample Preparation

Crystals of bsNOS and bsNOS I218V were obtained as previously described[12,15]. Protein crystals were slowly cryoprotected in the presence of 2 mM H_4B and 25% v/v glycerol as previously reported[12]. Following cryoprotection, the crystals were soaked in the presence of 5–10 mM of the corresponding NOS inhibitor for 3–5 hours and then flash frozen using $N_2(l)$.

X-Ray Data Collection and Processing

X-ray diffraction data sets were collected on individual crystals at both the Advanced Light Source (Berkeley, CA) and the Stanford Synchrotron Radiation Light source (Palo Alto, CA). Data frames were indexed and integrated using either MOSFLM[18] or XDS[19]. The indexed data sets were scaled with Aimless[20] and some datasets with strong anisotropy were further scaled using the diffraction anisotropy server[21]. Structure factors were initially

refined using Refmac[22] and PHENIX[23] was used for later rounds of refinement. The program COOT[24] was used to model inhibitor binding, and PyMOL (Version 1.5.0.4 Schrödinger, LLC.) was used to generate figures. Data collection and refinement statistics are provided in Table S1.

Chemical Synthesis of 1, 2, and 11

tert*-Butyl (3-Hydroxybenzyl)(methyl)carbamate (19)—Step 1*. Methylamine in THF (4.1 mL, 8.24 mmol) was diluted with $CHCl_3$ (10 mL), and aldehyde **18** (0.500 g, 4.12 mmol) was added in a solution of $CHCl_3$/MeOH (10:1, 5 mL). Anhydrous sodium sulfate (~2 g) was added, and the mixture was stirred rapidly under an argon atmosphere at room temp for 90 min. Glacial AcOH (50 μL) an additional anhydrous sodium sulfate (~1 g) was then added. The mixture was stirred for a total of 4 h, and the sodium sulfate was filtered from the mixture. The filtrate was concentrated, and the residue was diluted with MeOH (20 mL) and cooled to 0 °C. $NaBH_4$ (0.203 g, 5.36 mmol) was added, and the mixture was warmed to room temp and stirred for 20 min. The resulting mixture was concentrated, and the residue was partitioned between EtOAc and sat. aq. $NaHCO_3$ (30 mL each). The layers were separated and the aqueous layer was extracted with EtOAc until no residual amine could be extracted (as measured by TLC). The organic layer was washed with sat. aq. NaCl (50 mL) and dried. Concentration afforded the intermediate secondary amine as an oil. *Step 2*. This amine was immediately diluted in THF (30 mL) and Boc_2O (0.900 g, 4.12 mmol) was added as a solution in minimal THF. The mixture was stirred at room temp for 3.5 h and then concentrated. The residue was partitioned between EtOAc and sat. aq. $NaHCO_3$ (30 mL each), the layers were separated, and the aqueous layer was extracted with EtOAc (3 × 30 mL). The combined organic layers were washed with H_2O and sat. aq. NaCl (50 mL each), dried over anhydrous sodium sulfate, and evaporated. The residue was purified by flash column chromatography (SiO_2), eluting with a gradient of hexanes to 35% EtOAc in hexanes to yield the product as a colorless syrup (0.756 g, 77%) that was used without further purification. ^{1}H-NMR (500 MHz; $CDCl_3$): δ 9.28 (br s, 1 H), 7.24-7.21 (m, 1 H), 7.09 (dd, J = 7.4, 1.6 Hz, 1 H), 6.94 (d, J = 8.1 Hz, 1 H), 6.81 (t, J = 7.4 Hz, 1 H), 4.31 (s, 2 H), 2.88 (s, 3 H), 1.48 (s, 9 H); ^{13}C-NMR (126 MHz; $CDCl_3$): δ 156.4, 131.4, 130.1, 122.6, 119.3, 117.7, 81.6, 49.6, 34.1, 28.5.

7-[(2-((Methylamino)methyl)phenoxy)methyl]quinolin-2-amine Dihydrochloride (11)—NaH (60% suspension in mineral oil, 0.011 g, 0.27 mmol) was diluted with anhydrous DMF (1.5 mL) and cooled to 0 °C under an argon atmosphere. A solution of phenol **19** (0.064 g, 0.27 mmol) in anhydrous DMF (1.5 mL) was added slowly to the suspension and stirred at 0 °C for 20 min, followed by addition of bromide **20** (see[25]; 0.075 g, 0.27 mmol) in anhydrous DMF. The reaction mixture was stirred at 0 °C for 1 h and was then quenched by addition of a 1:1 sat. aq. NaCl/H_2O (~15 mL). The mixture was extracted with EtOAc (3 × 20 mL), and the organic phase was washed with 5% aq. NaCl (3×50 mL) and sat aq. NaCl (50 mL). The organic layer was dried over anhydrous sodium sulfate, concentrated, and purified by flash column chromatography (SiO_2), eluting with a gradient of 5% EtOAc in CH_2Cl_2 to 35% EtOAc in CH_2Cl_2 to yield acetamide **21** as an off-white foam (0.099 g, 85%), which was immediately deprotected. Compound **21** was diluted with anhydrous MeOH (10 mL), and anhydrous K_2CO_3 (0.063 g, 0.457 mmol) was added. The

mixture was heated at reflux for 2.5 h, cooled, and concentrated. The resulting residue was partitioned between EtOAc and 1:1 H_2O/sat. aq. NaCl, and the aqueous layer was extracted with EtOAc (3 × 20 mL). The organic layers were washed with sat. aq. NaCl (40 mL), dried over anhydrous sodium sulfate, and concentrated. EtOAc (2 mL) was added to the residue, followed by hexanes (15 mL). The mixture was heated to boiling, and sonicated vigorously until an off-white solid precipitate formed, which was collected by filtration and washed with hexanes. This free aminoquinoline was diluted in 10:1 ether/MeOH, and filtered to remove any particulate matter. To the filtered solution was added methanolic HCl (3 M, 1 mL), and the mixture was stirred at room temperature overnight. The resulting precipitate was collected, diluted in hot MeOH (1 mL), and ether (10 mL) was added, giving **11** as a white flocculent solid (0.063 g, 75%) after washing with ether: mp 284–286 °C. ^{1}H-NMR (500 MHz; DMSO-d_6): δ 14.50 (br s, 1 H), 9.30 (br s, 1 H), 8.99 (br s, 2 H), 8.37 (d, J = 9.2 Hz, 2 H), 8.30 (br s, 1 H), 7.95 (d, J = 8.2 Hz, 1 H), 7.91 (s, 1 H), 7.60 (d, J = 7.6 Hz, 1 H), 7.49 (dd, J = 7.5, 1.6 Hz, 1 H), 7.43-7.39 (m, 1 H), 7.17 (d, J = 8.1 Hz, 1 H), 7.09 (d, J = 9.3 Hz, 1 H), 7.05 (td, J = 7.4, 0.7 Hz, 1 H), 5.41 (s, 2 H), 4.21 (t, J = 5.5 Hz, 2 H), 2.62 (t, J = 5.2 Hz, 3 H); ^{13}C-NMR (126 MHz; DMSO-d_6): δ 156.1, 154.4, 142.8, 142.0, 131.4, 130.8, 128.9, 123.6, 121.0, 120.3, 120.2, 115.1, 113.7, 112.5, 68.6, 46.4, 32.6; one of the aminoquinoline carbons is not visible due to baseline broadening. ESIMS *m/z* (rel. intensity) 294 (MH^+, 100); HRMS calcd for $C_{18}H_{20}N_3O^+$: 294.1601; found, 294.1612. HPLC purity: 100%.

Quinolin-2-amine Hydrochloride (1)—A sealable vial was charged with 2-chloroquinoline (**22**, 0.244 g, 1.5 mmol), $Pd_2(dba)_3$ (13 mg), and DavePhos (13 mg). Anhydrous dioxane (1.1 mL) and LHMDS (1 M in THF, 3.4 mL, 3.4 mmol) were added, the solution was purged with argon, and the vial was sealed. The mixture was heated to 100 °C for 20 h, and then cooled and poured into 6 N HCl (20 mL). The solution was washed with EtOAc (20 mL), and the EtOAc layer was extracted with 6 N HCl (3 × 20 mL). The various aqueous layers were washed with EtOAc (2 × 30 mL). The EtOAc washes were discarded, and the combined aqueous phase was basified with NaOH to pH 12. The suspension was extracted with EtOAc (3 × 30 mL), and the organic layers were washed with 5% aq. NaCl and sat. aq. NaCl (50 mL each), dried over anhydrous sodium sulfate, and concentrated. The residue was purified by flash column chromatography (SiO_2), eluting with a gradient of EtOAc to 2% MeOH in EtOAc to yield a white solid after dissolving in EtOAc (5 mL) and precipitating with hexanes (50 mL). The collected solid was diluted with dry ether (8 mL) and treated with methanolic HCl (3 M, 1.5 mL, 4.5 mmol), upon which a colorless solid precipitated, which was collected by filtration and dried to afford **1** (0.150 g, 70%): mp 110–111 °C (softens, possibly free-bases); 120–122 °C (melts) (see[26] mp: 222–223 °C (HCl salt); 126–127 °C (free-base)). ^{1}H-NMR (500 MHz; DMSO-d_6): δ 14.28 (s, 1 H), 9.14 (s, 1 H), 8.38 (d, J = 9.3 Hz, 1 H), 8.21 (br s, 1 H), 7.92 (dd, J = 8.0, 1.0 Hz, 1 H), 7.77 (td, J = 7.7, 1.3 Hz, 1 H), 7.71 (d, J = 8.2 Hz, 1 H), 7.50-7.47 (m, 1 H), 7.12 (d, J = 9.3 Hz, 1 H); ^{13}C-NMR (126 MHz; DMSO-d_6): δ 154.3, 143.0, 135.7, 132.5, 128.8, 124.9, 120.9, 117.2, 113.8. ESIMS *m/z* (rel. intensity) 145 (MH^+, 100). HPLC purity: 99.6%.

4-Methylquinolin-2-amine Hydrochloride (2)—A mixture of 2-chlorolepidine (**23**) (0.300 g, 1.69 mmol), K_2CO_3 (1.17 g, 8.45 mmol), and dry acetamide (8.0 g, 135 mmol)

was heated to 240 °C for 2 h, during which time a yellow color formed. The solution was then cooled and poured into H_2O (50 mL). The suspension was extracted with EtOAc (3 × 50 mL), and the organic layer was washed with H_2O (3 × 50 mL) and sat. aq. NaCl (50 mL) and then dried over anhydrous sodium sulfate. The solution was concentrated and the residue was purified by flash column chromatography (SiO_2), eluting with a gradient of EtOAc to 2% MeOH in EtOAc to yield a yellow solid after washing with 2% EtOAc in hexanes. The solid was diluted with dry ether (8 mL) and treated with methanolic HCl (3 M, 1.5 mL, 4.5 mmol), precipitating a colorless solid. An analytically pure sample was produced by preparative HPLC, using an Agilent Infinity 1200 HPLC pump with MS SQ 6130 detector, with a Phenomenex Gemini 5μ C18 150×21.2 mm column, eluting with a gradient of 97% H_2O (+ 0.1% formic acid) + 3% MeCN (+ 0.1% formic acid) to 40% H_2O (+ 0.1% formic acid) + 60% MeCN (+ 0.1% formic acid) over 20 min, at a flow rate of 20 mL/min. The product was obtained as a white solid (87 mg, 33%): mp 199–201 °C (see[27] mp 201–202 °C)); ^{1}H-NMR (500 MHz; DMSO-d_6): δ 14.04 (s, 1 H), 8.94 (br s, 1 H), 8.30 (br s, 1 H), 8.00 (dd, J = 8.2, 1.0 Hz, 1 H), 7.78 (ddd, J = 8.3, 7.1, 1.3 Hz, 1 H), 7.70 (dd, J = 8.3, 0.7 Hz, 1 H), 7.51 (ddd, J = 8.2, 7.1, 1.2 Hz, 1 H), 6.95 (d, J = 1.0 Hz, 1 H), 2.63 (d, J = 1.0 Hz, 3 H); ^{13}C-NMR (126 MHz; DMSO-d_6): δ 153.6, 152.4, 135.5, 132.3, 125.4, 124.8, 121.1, 117.5, 112.6, 19.0; ESIMS *m/z* (rel. intensity) 159 (MH^+, 100). HPLC purity: 100%.

Results and Discussion

Spectral Binding Analysis

Although the various NOS isoforms have very similar active site structures, one potentially important difference between mammalian and bacterial NOS isoforms is that an L-Ile in bNOS, which is a L-Val in mNOS isoforms, interacts with hydrophobic portions of inhibitors. Previously, we postulated that this subtle difference in hydrophobicity might contribute to inhibitor selectivity for bNOS[1]. To further evaluate the role of the bNOS Ile residue, we performed mutagenesis studies in bsNOS and the reverse mutation studies in iNOS. From the 17 aminoquinoline inhibitors studied here, Ile-218 was observed to contribute to the bsNOS inhibitor specificity (Table 1) as noted by an increase in K_s for the I218V bsNOS mutant. Specifically, for both **1** and **2** we observed a 26-fold and 7-fold decrease in inhibitor specificity between WT and I218V, respectively. However, this trend was not consistently observed for the K_s measured in iNOS WT and V352I iNOS. In fact, the K_s only decreased for compounds **7**, **8**, **13**, and **14** when V352I was introduced in iNOS and increased for 10 of the other inhibitors.

Aminoquinoline Inhibition of bNOS

The two most potent bsNOS inhibitors identified by K_S analysis (**1** and **2**, Table 1), were also the simplest aminoquinolines studied. To further evaluate the relationship between Ile218 and the inhibitory potential of aminoquinolines, both **1** and **2** were evaluated using the previously described bBiDomain assay[15]. The bBidomain is a construct consisting of the *B. subtilis* flavodoxin, YkuN, fused to the C-terminal end of bsNOS. In the presence of the *B. subtilis* FAD-containing reductase, YumC. and NADPH the bBidomain oxidizes substrate much more rapidly than the 3 component system consisting of bsNOS, YkuN, and YumC.[15] This has provided a more facile method for rapidly screening the ability of inhibitors to

block bsNOS activity.[1] Both of these compounds were found to have IC_{50} values in the low μM range (Table 2). From these studies we also found that introduction of I218V to bBiDomain resulted in a small increase in the measured IC_{50} values.

Crystal Structure Analysis

Although 22 crystal structures were solved, we focus here on those that provide the most important insights into the effect of the I218V mutation. As expected, in all of these structures the aminoquinoline forms stacking interactions with the heme group and hydrogen bonds with the conserved active site Glu243, and it directly contacts Ile218 through a van der Waals interaction (Fig, 2, Fig. S1). For the simplest inhibitors, **1** and **2**, the 8–27 fold decrease in binding affinity in the I218V bsNOS mutant can be rationalized based on the additional non-covalent interactions between Ile218 and the inhibitor compared to Val218. We estimated the additional stability of the larger Ile vs. Val by calculating the non-bonded interaction energy between the inhibitor and residue 218 using the Sander module in Amber. The WT Ile provides an additional −1.8 kcal/mol greater stability. This is in agreement with the ΔG obtained from the spectral K_s data (≈−2 kcal/mol).

The addition of a linker to the aminoquinoline with various tail groups results in various binding orientations of the inhibitor tail, which extends out of the active site. The inhibitor tail binds better for some inhibitors than others as judged by the electron density. For example, the electron densities observed for the tail end of inhibitors **6** and **8** are well ordered, while those for inhibitors **10** and **13** are not (Fig. 2). There is also a relationship between how well ordered the tail end of the inhibitor is and the effect of the I218V mutant on binding affinity. For example, both inhibitors **6** and **8** were found to have well-defined electron density throughout. The more well-defined electron density inhibitors, such as **6** and **8**, were also minimally perturbed by the I218V mutation on the basis of differences in K_S (Table 1). In contrast, inhibitors with less defined inhibitor electron density, such as **10** and **13**, have K_S differences of 8 and 120 fold, respectively, between WT and I218V bsNOS (Table 1). We postulate that for inhibitors **10** and **13** the tail end of the inhibitor does not contribute much to stability so the effect of the mutation on binding to the aminoquinoline part of the inhibitor is more pronounced. Conversely, the effect of the mutant is less pronounced for **6** and **8** since the tail end contributes more to inhibitor binding. This results in a decreased effect on the mutation on the aminoquinoline portion of the inhibitor. One reason **6** and **8** have a more ordered tail is due to the interaction of the secondary amino group with the heme propionates.

Since the I218V mutation has a large effect on the K_S of inhibitor **13**, the crystal structure of the mutant enzyme bound to **13** was also solved (Figure 2). In the mutant, the tail end of the inhibitor exhibits weak density, and the F_o-F_c maps indicate that the tail of the inhibitor occupies at least two orientations. An important difference between **13** and some of the other inhibitors is that the linker in **13** has an ether oxygen rather than a secondary amino group. As a result, the linker of **13** cannot form a H-bond with the heme propionate, while the secondary amino group of inhibitors like **8** can form a hydrogen bond. Given the extra interactions in **8**, the I218V mutation has little effect, while for **13**, with no linker H-bonding

possibilities, the effect of the destabilizing I218V mutation is much larger because the aminoquinoline itself contributes more to overall binding.

One remaining question is why the I218V mutation has a large effect on K_S in bsNOS but the reverse mutation in iNOS, V352L, has little effect. For example, the I218V mutation decreases affinity for inhibitor **13** by approximately 120 fold in bsNOS but there is little difference between WT iNOS and the V352I mutant. There are, however, other differences in the active site between bsNOS and iNOS. For example, His128 in bsNOS is replaced by Ala in iNOS. His128 contacts both the central region of the larger inhibitors as well as Ile218 thereby restricting inhibitor mobility within the binding pocket. The bsNOS active site is also more open than the iNOS active site because, unlike iNOS, bsNOS does not contain an N-terminal Zn^{2+} binding motif. Previously, we have observed that the open pterin site of bsNOS accommodates the binding of aminopyridine-based inhibitors[12] and allows for the binding modes of thiophenecarboximidamide-based inhibitors that are unique to bsNOS[3]. Therefore, it is likely that the N-terminal binding motif in iNOS also influences the binding of the longer aminoquinoline inhibitors that extend out of the active site in bsNOS.

Initial structural studies of aminoquinolines binding to bsNOS indicated that they might bind to the pterin site (data not shown). To determine if aminoquinolines can bind to this site we prepared crystals of **6** and **16** without H_4B present during the cryosoak. Processing of the crystallographic data provided a two-site binding model of both **6** and **16** to bsNOS when H_4B is absent (Figures 3B and 3D). In these two site models, one inhibitor is bound at the active site and the second binds to the pterin site by forming a **π-π** stacking interaction with Trp329. In the case of **6**, inhibitor binding at the pterin site requires a water molecule to bridge a hydrogen bond to the heme propionate group. Binding of **6** is further stabilized by a salt bridge between the secondary linker amine of **6** and R344(C=O) at the dimer interface (Figure 3B). Unlike **6**, a hydrogen bond between inhibitor linker and R344(C=O) is not observed with **16** because it has an ether-linked tail (Figure 3D). On the basis of $2F_o$-F_c maps, the binding of both **6** and **16** to the pterin site is weak compared to binding of H_4B, as H_4B can easily out-compete the aminoquinoline inhibitors evaluated. Inspection of both **6** and **16** bound to the active site reveals the binding mode to be unchanged regardless of the ligand present at the pterin site (Figure 3). This confirms our earlier observations that the aminopyridine of inhibitors prefer the pterin site over aminoquinolines[12]. Even in the presence of H_4B we have found that aminopyridines can be quite effective at displacing H_4B while aminoquinolines prefer the active site[12].

Conclusions

Aminoquinoline-based inhibitors have been developed to inhibit NOS activity. Since the aminoquinoline scaffold also has been previously found to function as an antimicrobial agent against the highly pathogenic organism MRSA[1], an improved understanding of aminoquinoline binding to bNOS was necessary to further drug design efforts and identify new scaffolds for inhibitor design. Previous evidence also indicates that the potency and specificity afforded by the aminoquinoline-based inhibitors to be controlled by the subtle differences in hydrophobicity at the bNOS active site[1]. Specifically, the hydrophobic patch contributed by Ile-218 (mNOS equivalent residue is Val) allows for tighter binding of the

aminoquinoline group as a result of a van der Waals interaction between the aminoquinoline group and active site Ile-218 residue.

On the basis of these results one might have anticipated that the reverse mutation in iNOS, V352I, should improve binding, but there is little difference between WT and mutant. However, in bsNOS His218 contacts the inhibitor while this equivalent residue is an L-Ala in iNOS and a L-Ser in both *H. sapiens* endothelial NOS (eNOS) and neuronal NOS (nNOS), respectively. As a result, the active site of bsNOS provides more contacts with the aminoquinoline inhibitors. These results, combined with previous studies, indicate at least two structural and functional differences between bNOS and mNOS that can be exploited in the design of bNOS-selective inhibitors. First, the larger aminoquinoline compared to the smaller aminopyridine favors the bNOS active site owing to the more extensive nonbonded contacts provided by Ile218. Second, aminopyridines favor the pterin site over aminoquinolines. Targeting the pterin site might be especially useful since pterins bind more weakly to bNOS than nNOS, which should result in easier displacement of H_4B by inhibitors in bNOS. Thus, an inhibitor with an aminoquinoline in the active site and an aminopyridine in the pterin site has the potential to be an especially potent and selective bNOS inhibitor.

Supplementary Material

Refer to Web version on PubMed Central for supplementary material.

Acknowledgments

This work is greatly indebted to the expertise and wisdom provided by Dr. Huiying Li. We are also very grateful to the beamline staff at both the Advanced Light Source and the Stanford Synchrotron Radiation Light source (Palo Alto, CA) for help with remote data collection. This work was supported by National Institute of Health grants GM57353 (to TLP), GM49725 (to RBS), and F32GM109667 (to MAC).

This work was supported by NIH grant GM57353 (TLP) and NIH grant GM49725 (to RBS).

Abbreviations

NOS	nitric oxide synthase
NO	nitric oxide
L-Arginine	L-Arg
nNOS	neuronal nitric oxide synthase
eNOS	endothelial nitric oxide synthase
iNOS	inducible nitric oxide synthase
mNOS	mammalian nitric oxide synthase
bNOS	bacterial nitric oxide synthase
bsNOS	*Bacillus subtilis* nitric oxide synthase

saNOS	*Staphylococcus aureus* nitric oxide synthase
MRSA	methicillin-resistant *Staphylococcus aureus*

References

1. Holden JK, Kang S, Beasley FC, Cinelli MA, Li H, Roy SG, Dejam D, Edinger AL, Nizet V, Silverman RB, Poulos TL. Nitric Oxide Synthase as a Target for Methicillin-Resistant Staphylococcus aureus. Chem. Biol. 2015; 22:785–792. [PubMed: 26091171]
2. Crane BR, Sudhamsu J, Patel BA. Bacterial Nitric Oxide Synthases. Annu. Rev. Biochem. 2010; 79:445–470. [PubMed: 20370423]
3. Holden JK, Dejam D, Lewis MC, Huang H, Kang S, Jing Q, Xue F, Silverman RB, Poulos TL. Inhibitor Bound Crystal Structures of Bacterial Nitric Oxide Synthase. Biochemistry. 2015; 54:4075–4082. [PubMed: 26062720]
4. Wang ZQ, Lawson RJ, Buddha MR, Wei CC, Crane BR, Munro AW, Stuehr DJ. Bacterial flavodoxins support nitric oxide production by Bacillus subtilis nitric-oxide synthase. J. Biol. Chem. 2007; 282:2196–2202. [PubMed: 17127770]
5. Pant K, Crane BR. Structure of a loose dimer: an intermediate in nitric oxide synthase assembly. J. Mol. Biol. 2005; 352:932–940. [PubMed: 16126221]
6. Adak S, Bilwes AM, Panda K, Hosfield D, Aulak KS, McDonald JF, Tainer JA, Getzoff ED, Crane BR, Stuehr DJ. Cloning, expression, and characterization of a nitric oxide synthase protein from Deinococcus radiodurans. Proc. Natl. Acad. Sci. U.S.A. 2002; 99:107–112. [PubMed: 11756668]
7. Pant K, Bilwes AM, Adak S, Stuehr DJ, Crane BR. Structure of a nitric oxide synthase heme protein from Bacillus subtilis. Biochemistry. 2002; 41:11071–11079. [PubMed: 12220171]
8. Sudhamsu J, Crane BR. Bacterial nitric oxide synthases: what are they good for? Trends Microbiol. 2009; 17:212–218. [PubMed: 19375324]
9. Gusarov I, Nudler E. NO-mediated cytoprotection: instant adaptation to oxidative stress in bacteria. Proc. Natl. Acad. Sci. U.S.A. 2005; 102:13855–13860. [PubMed: 16172391]
10. Gusarov I, Shatalin K, Starodubtseva M, Nudler E. Endogenous nitric oxide protects bacteria against a wide spectrum of antibiotics. Science. 2009; 325:1380–1384. [PubMed: 19745150]
11. van Sorge NM, Beasley FC, Gusarov I, Gonzalez DJ, von Kockritz-Blickwede M, Anik S, Borkowski AW, Dorrestein PC, Nudler E, Nizet V. Methicillin-resistant Staphylococcus aureus bacterial nitric-oxide synthase affects antibiotic sensitivity and skin abscess development. J. Biol. Chem. 2013; 288:6417–6426. [PubMed: 23322784]
12. Holden JK, Li H, Jing Q, Kang S, Richo J, Silverman RB, Poulos TL. Structural and biological studies on bacterial nitric oxide synthase inhibitors. Proc. Natl. Acad. Sci. U.S.A. 2013; 110:18127–18131. [PubMed: 24145412]
13. Holden JK, Kang S, Hollingsworth SA, Li H, Lim N, Chen S, Huang H, Xue F, Tang W, Silverman RB, Poulos TL. Structure-based design of bacterial nitric oxide synthase inhibitors. J. Med. Chem. 2015; 58:994–1004. [PubMed: 25522110]
14. Goldschmidt L, Cooper DR, Derewenda ZS, Eisenberg D. Toward rational protein crystallization: A Web server for the design of crystallizable protein variants. Protein Sci. 2007; 16:1569–1576. [PubMed: 17656576]
15. Holden JK, Lim N, Poulos TL. Identification of redox partners and development of a novel chimeric bacterial nitric oxide synthase for structure activity analyses. J. Biol. Chem. 2014; 289:29437–29445. [PubMed: 25194416]
16. Wang ZQ, Wei CC, Sharma M, Pant K, Crane BR, Stuehr DJ. A conserved Val to Ile switch near the heme pocket of animal and bacterial nitric-oxide synthases helps determine their distinct catalytic profiles. J. Biol. Chem. 2004; 279:19018–19025. [PubMed: 14976216]
17. Roman LJ, Sheta EA, Martasek P, Gross SS, Liu Q, Masters BS. High-level expression of functional rat neuronal nitric oxide synthase in Escherichia coli. Proc. Natl. Acad. Sci. U.S.A. 1995; 92:8428–8432. [PubMed: 7545302]

18. Battye TG, Kontogiannis L, Johnson O, Powell HR, Leslie AG. iMOSFLM: a new graphical interface for diffraction-image processing with MOSFLM. Acta. Crystallogr. D. 2011; 67:271–281. [PubMed: 21460445]
19. Kabsch W. Xds. Acta. Crystallogr. D. 2010; 66:125–132. [PubMed: 20124692]
20. Evans P. Scaling and assessment of data quality. Acta. Crystallogr. D. 2006; 62:72–82. [PubMed: 16369096]
21. Strong M, Sawaya MR, Wang S, Phillips M, Cascio D, Eisenberg D. Toward the structural genomics of complexes: crystal structure of a PE/PPE protein complex from Mycobacterium tuberculosis. Proc. Natl. Acad. Sci. U.S.A. 2006; 103:8060–8065. [PubMed: 16690741]
22. Murshudov GN, Vagin AA, Dodson EJ. Refinement of macromolecular structures by the maximum-likelihood method. Acta. Crystallogr. D. 1997; 53:240–255. [PubMed: 15299926]
23. Adams PD, Afonine PV, Bunkoczi G, Chen VB, Davis IW, Echols N, Headd JJ, Hung LW, Kapral GJ, Grosse-Kunstleve RW, McCoy AJ, Moriarty NW, Oeffner R, Read RJ, Richardson DC, Richardson JS, Terwilliger TC, Zwart PH. PHENIX: a comprehensive Python-based system for macromolecular structure solution. Acta. Crystallogr. D. 2010; 66:213–221. [PubMed: 20124702]
24. Emsley P, Lohkamp B, Scott WG, Cowtan K. Features and development of Coot. Acta. Crystallogr. D. 2010; 66:486–501. [PubMed: 20383002]
25. Cinelli MA, Li H, Chreifi G, Martasek P, Roman LJ, Poulos TL, Silverman RB. Simplified 2-aminoquinoline-based scaffold for potent and selective neuronal nitric oxide synthase inhibition. J. Med. Chem. 2014; 57:1513–1530. [PubMed: 24472039]
26. Rudner, B. Process for aminating nitrogen-containing heterocyclic compounds. US Patent. 2892841 A. 1959.
27. Kaye IA. 2-Lepidyl Substituted Diamines. J. Am. Chem. Soc. 1949; 71:2322–2325.
28. Cinelli MA, Li H, Pensa AV, Kang S, Roman LJ, Martasek P, Poulos TL, Silverman RB. Correction to Phenyl Ether- and Aniline-Containing 2-Aminoquinolines as Potent and Selective Inhibitors of Neuronal Nitric Oxide Synthase. J. Med. Chem. 2016; 59:1246. [PubMed: 26807481]

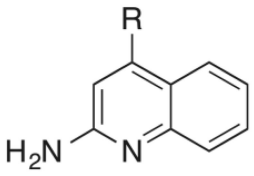

1. R=H
2. R=CH_3

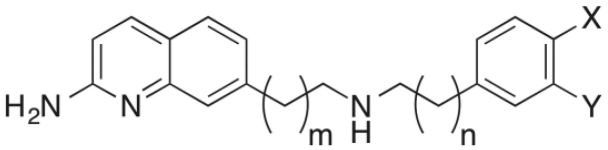

3. m=0, n=1, X=F, Y=H
4. m=0, n=2, X=H, Y=F
5. m=1, n=0, X=F, Y=H
6. m=1, n=1, X=H, Y=F
7. m=1, n=2, X=F, Y=H
8. m=0, n=0, X= H, Y= $N(CH_3)_2$

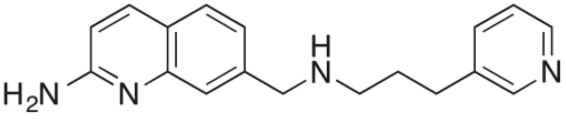

9.

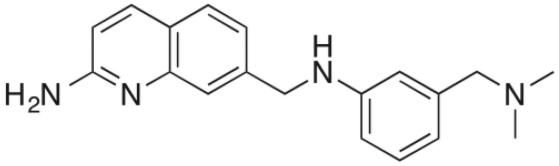

10.

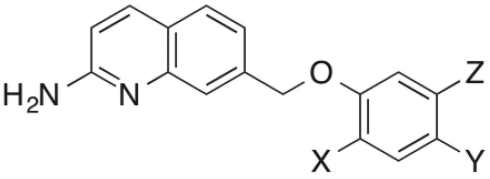

11. X=CH_2NHCH_3, Y=H, Z=H
12. X=H, Y=H, Z=CH_2NHCH_3
13. X=H, Y=H, Z=$CH_2CH_2NHCH_3$
14. X=H, Y=Cl, Z=$CH_2CH_2NHCH_3$
15. X=H, Y=H, Z=CH_2NH_2
16. X=H, Y=$CH_2N(CH3)_2$, Z=H

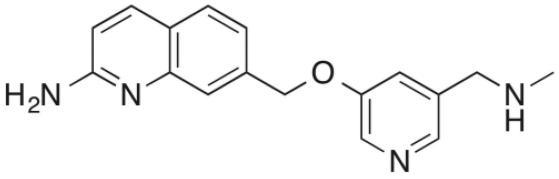

17.

Figure 1.

NOS inhibitors reported in this study. Chemical syntheses of inhibitors **1**, **2**, and **11** are reported here (see Experimental Procedures). Syntheses of **3–7** are reported in[25] and that of **8** and **9** are reported in http://patents.justia.com/patent/9212144. Syntheses of inhibitors **10** and **12–17** are reported in[28].

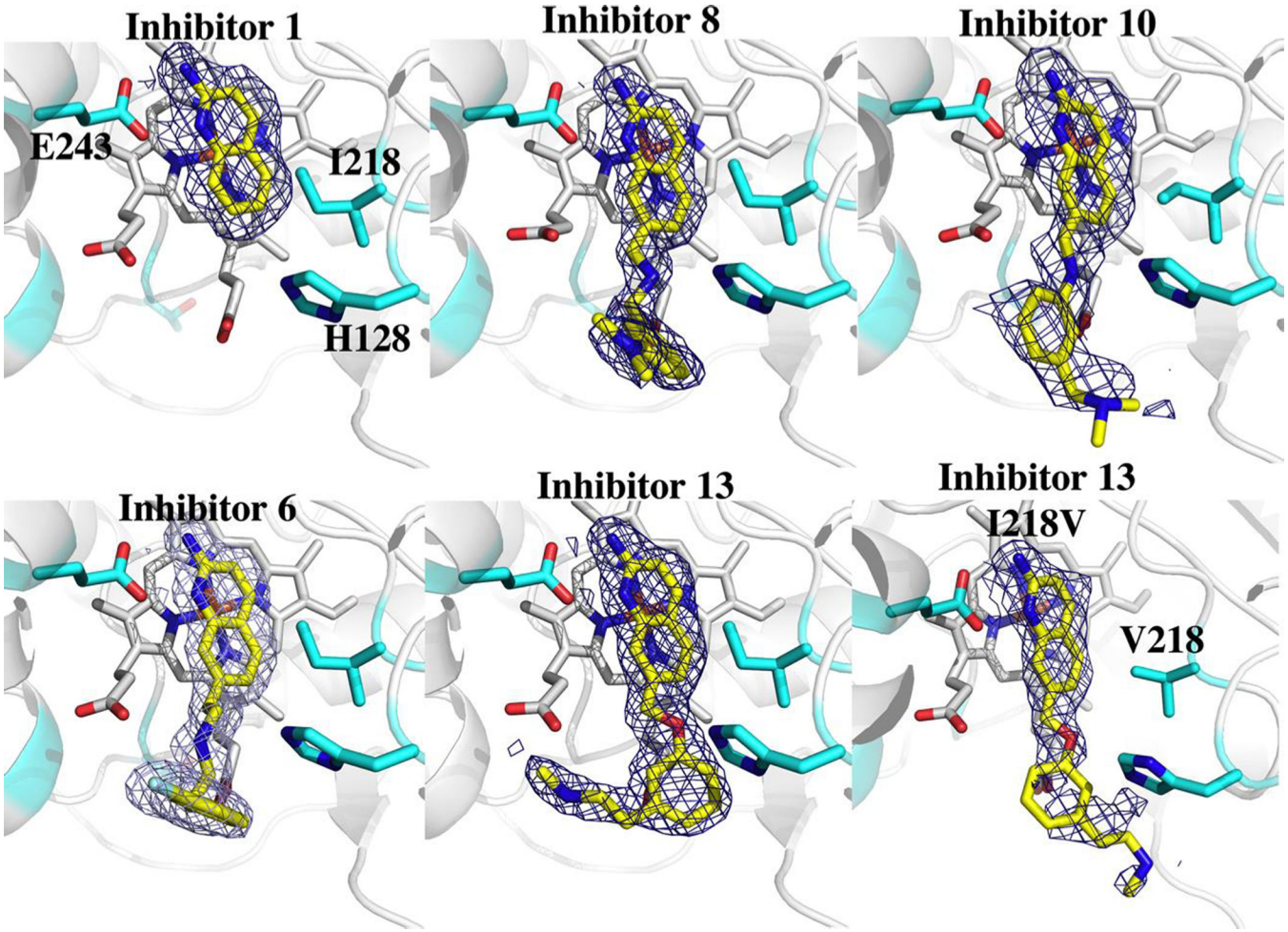

Figure 2.

Crystal structures of WT and I218V bsNOS complexed with inhibitors shown in yellow and a F_o-F_c map contoured at 1.0σ. The aminoquinoline group binds to the NOS active site for all molecules through a hydrogen bond to E243. The tails of inhibitors **6**, **8**, and **10** are stabilized by hydrogen bonds to heme propionate. **13** contains an ether group that positions the inhibitor tail away from the heme propionate group because of electrostatics.

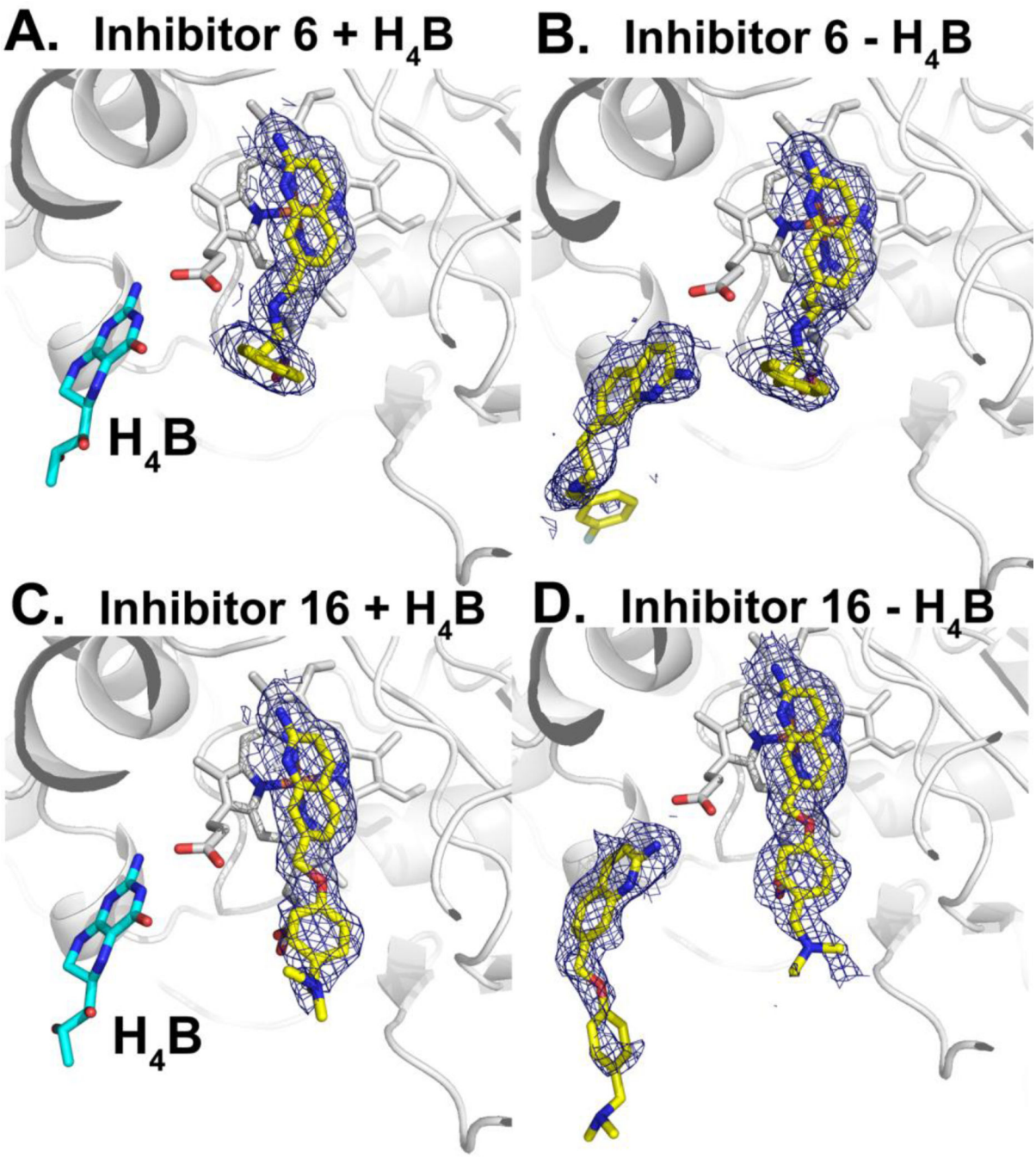

Figure 3.

$2F_o$-F_c maps contoured at 1 σ for inhibitors **6** and **16** both in the presence and absence of H_4B. Inhibitors are colored yellow and H_4B is shown as cyan. When H_4B is absent inhibitor binding is also observe at the pterin site for B) **6** and D) **16**.

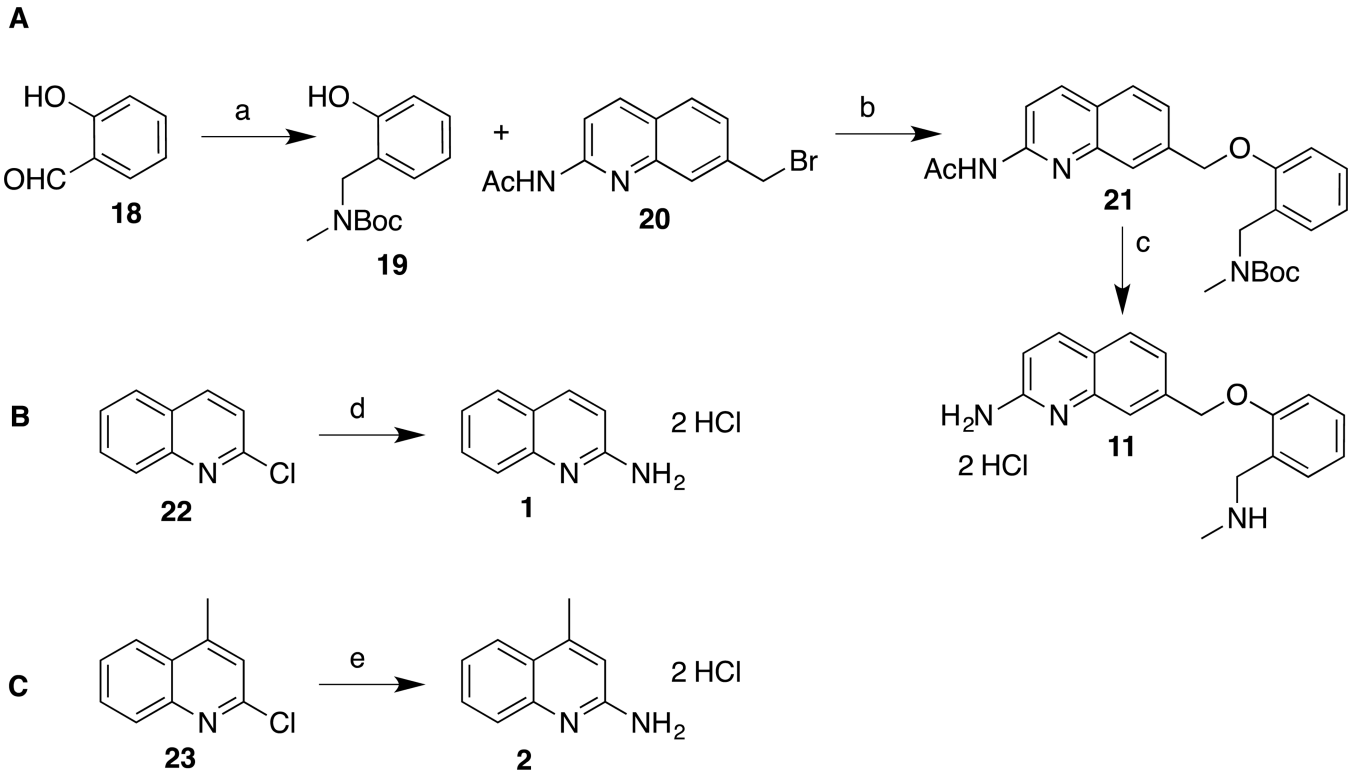

Scheme 1. Synthetic Route to 1, 2, and 11

Reagents and conditions: (a) *i.* $MeNH_2$ in THF, cat. AcOH, $CHCl_3$/MeOH, Na_2SO_4, r.t., *ii.* $NaBH_4$, MeOH, 0 ° C - r.t., *iii.* Boc_2O, THF, r.t.; (b) *i.* Phenol **19**, NaH, DMF, 0 ° C, *ii.* **20** (in DMF), 0 ° C; (c) *i.* K_2CO_3, MeOH, reflux, *ii.* HCl/MeoH, ether, r.t., after isolation; (d) *i.* LHMDS in THF, Pd_2dba_3, DavePhos, dioxane, 100 °C, *ii.* HCl/MeOH, ether, r.t., after isolation; (e) *i.* $AcNH_2$, K_2CO_3, 240 ° C, *ii.* HCl/MeOH, ether, r.t., after isolation.

Table 1

Spectral binding constants for inhibitors against NOS isoforms and mutants.

Ligand	bsNOS WT K_S (μM)	bsNOS I218V K_S (μM)	Human iNOS K_S (μM)	Human iNOS V352I K_S (μM)
L-Arg	4.8 ± 0.1[a]	2.0 ± 0.2[a]	16.1 ± 0.7[a]	40.9 ± 4.3[a]
1	1.25 ± 0.03	33.3 ± 1.5	4.5 ± 0.5	11.1 ± 0.7
2	0.80 ± 0.08	6.1 ± 0.3	3.5 ± 0.2	14 ± 1
3	3.2 ± 0.1	41 ± 6	7.1 ± 1.2	50 ± 18
4	3.2 ± 0.1	97 ± 6	91 ± 5	76 ± 6
5	1.3 ± 0.1	31 ± 2	40 ± 6	40 ± 3
6	6.7 ± 0.7[β]	12 ± 1[β]	42 ± 8	43 ± 5
7	3.6 ± 0.8[β]	18 ± 2	70 ± 35	50 ± 9
8	14.1 ± 0.4	11 ± 3	107 ± 39	80 ± 19
9	2.0 ± 0.1	34 ± 3	34 ± 4	44 ± 4
10	19 ± 1	154 ± 12	14 ± 3	36 ± 11
11	7.5 ± 0.3	182 ± 39	18 ± 2	33 ± 11
12	3.4 ± 0.1	266 ± 100	11 ± 1	56 ± 9
13	2.7 ± 0.1	320 ± 140	140 ± 29	122 ± 16
14	3.0 ± 0.1	39 ± 2	39 ± 3	26 ± 2
15	2.2 ± 0.1	184 ± 35	61 ± 6	61 ± 7
16	3.4 ± 0.1	103 ± 22	67 ± 14	117 ± 20
17	1.3 ± 0.1	17 ± 2	2.8 ± 0.3	8.3 ± 1.5

[a] Value reported in,[16]

[β] Value reported in.[1]

Table 2

IC_{50} (μM) of aminoquinoline inhibitors evaluated using bBidomain.

	WT	I218V
1	27.3	63.9
2	36.6	53.3